Nanostructural evolution of high loading Rh/lanthana catalysts through the preparation and reduction steps

S. Bernal[a], J.J. Calvino[a], C. López-Cartes[a], J.M. Pintado[a], J.A. Pérez-Omil[a],
J.M. Rodríguez-Izquierdo[a,*], K. Hayek[b], G. Rupprechter[b]

[a]*Departamento de Ciencia de los Materiales e Ingeniería Metalúrgica y Química Inorgánica, Universidad de Cádiz,*
Apartado 40, 11510, Puerto Real, Cádiz, Spain
[b]*Institut für Physikalische Chemie der Universität Innsbruck, Innrain 52a, A-6020, Innsbruck, Austria*

Abstract

A detailed high resolution electron microscopy investigation of different Rh/lanthana catalysts has been carried out. Samples prepared by wet impregnation using either aqueous or acetone solutions of rhodium nitrate and metal deposition by evaporation under high vacuum have been studied. The nanostructural evolution of the support and the metal phase through the different preparation steps has been tracked. Thus, the effects of reduction treatments in a wide range of temperatures (473–973 K) have been taken into consideration.

Scanning electron microscopy images evidence an intense dissolution of the lanthanide sesquioxide crystallites during the impregnation step with the rhodium nitrate aqueous solution. Such an effect could not be detected in the catalyst prepared using an acetone solution of the same metal precursor. On its hand, HREM indicates the presence of a highly dispersed metal phase in the catalyst prepared in water after reduction at low temperatures. Increasing the reduction temperature leads to a significant sintering of rhodium present both on the surface and the bulk of the support. Decorated rhodium particles are clearly visible in the three catalysts in the whole range of reduction temperatures. The drastic structural rearrangements which take place in the support during the reduction treatment and support dragging during sintering, are most likely the driving force for the decoration of the metal particle surfaces. © 1999 Elsevier Science B.V. All rights reserved.

Keywords: Supported metals; Rh; Lanthana; HREM; Metal–support interaction; Preparation; Microstructure

1. Introduction

Lanthanide sesquioxides, mainly lanthana, were profusely studied during the 1980s as catalytic supports of noble metal and as promoters of a variety of metal/SiO_2 and metal/Al_2O_3 catalysts. The high activity and, most important, the high selectivity towards C_1–C_2 oxygenate products shown by these catalysts in the CO hydrogenation reaction stimulated to a great extent this work, in which Pd [1–6], Rh [7–13], Ru [1–14] or Ni [1] catalysts supported or promoted by 4f-sesquioxides were investigated.

In some of these papers, metal–support interaction effects are claimed to be responsible of the singularities observed for these catalysts and structural models to explain this interaction are proposed in [15–18]. These models consider the existence of supported metal particles decorated on the surface with patches of material coming from the support, which would create synergetic sites for CO dissociation along a

---

*Corresponding author.

large metal–support interface. However, an analysis of these models reveals that important features are poorly defined.

It is striking, for example, that no explicit reference about the size of the particles is stated. A rough estimation can be obtained anyway. Thus, if a minimum extension of a few angstroms is assumed for the surface decorating patches, the diameters of the particles sketched in these models should be of a few nanometers. The difficulties found in the interpretation of chemisorption data observed for these catalysts may be at the roots of this imprecision. In effect, the occurrence of hydrogen spillover [9,10,19,20] and the strong inhibition of CO adsorption with respect to H_2 [10,12,16,20] poses some doubts about the calculation of average particle sizes from H/M or CO/M ratios.

Some controversies have risen also about the reduction state of the support in these patches and the mechanism by which they move up onto the metal particles. In the original proposals [15,16], lanthanide suboxide moieties produced during the reduction stage, at temperatures as low as 773 K, migrate on top of the metal particles located on the surface of the oxide support. More recently [10,17,18] the possibility of decoration by non-reduced species during the early stages of the preparation process, i.e. impregnation and drying, has been considered. Nevertheless no convincing evidence to support this last hypothesis has been reported.

The former interaction model is just a direct extrapolation of that proposed to explain the SMSI effect in titania-supported metal catalysts but ignores the chemical differences existing between TiO_2 and 4f-sesquioxides. The low reducibility of these sesquioxides [21] and their intrinsic base character are among the differences that should be taken into account. When the first difference is brought into consideration, a reduction process at low temperature seems an unlikely process to occur.

The influence of the basicity of the lanthanide sesquioxides on their properties as catalyst supports has been considered in detail in [20,22–26]. From the results contained in these papers two points are worth being highlighted: (1) the occurrence of a strong leaching effect of the support during the impregnation with the metal salt precursor solutions; (2) the severe chemical transformations of the support into a complex mixture of hydroxycarbonated phases. These

phenomena modify to a large extent the actual nature of the catalysts and can play an important role on the dispersion of the metal phase and as support migration mechanisms. In spite of their influence on the structure of the catalyst, none of these experimental facts has been considered in detail in the models referred above.

Different reports that appeared quite recently have renewed the interest in metal catalysts supported on lanthanide sesquioxides. In [27–33] it is shown that Ni and Rh catalysts supported on lanthana present interesting catalytic properties for the dry reforming of methane to syngas using CO_2. With respect to catalysts based on classic inert supports like SiO_2 or Al_2O_3, those based on La_2O_3 present a higher resistance to deactivation by coke. Moreover, for the latter an increase in catalytic activity is observed during the first hours of reaction. The promoting effect of lanthana has been once more attributed to metal–support interaction effects which involve the presence of reduced lanthanum species on the surface of the metal, in a clear reference to the models previously proposed in [15,16].

From these considerations it turns out that metal–support interaction effects in this family of catalysts are far from being well understood and that clarifying their origin still remains as a matter of, not only academic, but also of practical interest. It seems also reasonable that in systems like these, showing unconventional behavior and specific characterization problems, to obtain a clearer picture of these phenomena, the application of techniques which provide reliable information about the structure of the system is crucial.

High resolution electron microscopy (HREM) has proved to be a powerful technique to obtain direct information about the nanostructural features of metal–support interaction effects in M/TiO_2 [34–37] and M/CeO_2 catalysts [37–47]. The possibility of establishing in a direct way metal particles size distributions from HREM images [46,47], to observe the changes in the surface and bulk structure of the particles as a function of thermochemical treatments allows to retrieve structural information hardly accessible by means of other macroscopic techniques. On the basis of this information the temperature windows where different types of metal–support interaction mechanisms, like decoration [36,37,43] or alloying [45], which have been established are operating.

In this work, which extends and completes a previous one [48] done in our laboratory on Rh/Sm$_2$O$_3$ catalysts, HREM has been applied to study the structural evolution of a series of Rh supported on lanthana catalysts through the different steps involved in their preparation. Direct clues about the state of the metal phase throughout this process, the ways by which structural interactions are established with lanthana and the particular contribution of impregnation and reduction treatments to the actual nanostructure of the catalyst have been obtained. On the basis of the observations included here, an alternative model to account for metal–support interaction effects in this type of catalysts is proposed which is in better agreement with the well-known chemical properties of the 4f-oxides.

2. Experimental

Commercial, air stabilized, lanthana (Alfa Products, 99.9%, 10 m^2 g^{-1} BET) was employed for the preparation of two different Rh/lanthana catalysts by incipient wetness impregnation. One of them, with a 10% metal loading, was obtained by using a solution of Rh(NO$_3$)$_3$ in distilled water as impregnating agent. The metal salt was obtained from Alfa and contained a 35.6% Rh. In order to ascertain the role of the solvent during the impregnation step, a second catalyst was prepared using a solution of the same metal precursor in acetone instead of water. The final metal loading reached for these catalysts, after impregnation, was 8% Rh. Both catalysts were dried in an oven at 383 K for 10 h after the corresponding impregnation steps, and further stored in oxidized state in a desiccator.

Likewise, in order to avoid the influence of solvents during the impregnation, a third catalyst was prepared by high vacuum evaporation of Rh onto lanthana. Details about the experimental setup used for this preparation have been already described in [49]. In this case powder of air stabilized lanthana provided by Alfa was finely spread over the surface of a clean glass slide. The slide was placed inside the evaporation chamber and carefully pumped down. Afterwards Rh was deposited by electron beam bombardment of a pure rhodium rod at 1×10^{-5} Pa. The substrate temperature during evaporation was 298 K, the evaporation rate of the metal was about 1 Å min^{-1} and the nominal film thickness, as monitored by a quartz crystal oscillator, 8 Å. The chamber was subsequently vented and the powder collected and stored in a desiccator.

The reduction treatments were applied in pure hydrogen flowing at 60 cm^{-3} min^{-1} under atmospheric pressure. Ramps from room temperature up to the desired reduction temperature at a heating rate of 10 K min^{-1} have been used. Afterwards the samples were held at the reduction temperature for 1 h. Finally the gas flow was changed to helium, and the sample cooled down slowly in He and passivated as described in [43].

Details about the preparation of the electron microscopy specimens have been previously reported in [38]. High resolution electron microscopy (HREM) images and selected area electron diffraction patterns (SAED) have been obtained in a JEOL200-EX microscope operating at 200 kV. The structural resolution of this microscope, equipped with a side entry specimen holder and ionic pumping, is 0.21 nm.

The negatives were digitized using a conventional CCD camera, with a resolution of 768×512 pixels. Image processing and calculation of digital diffraction patterns (DDP) have been performed using the PC version of SEMPER 6+ software. The simulated images included in this work were obtained using the multislice routines of the EMS package [50] running on an Indy 4400-SC Silicon graphics work station. The structural models used as input for these calculations were built using the RHODIUS program developed in our lab [51].

The XRD diagrams presented in this work were obtained on a Siemens, model D-500. Radiation Cu K$_\alpha$ and a nickel filter were used.

3. Results

3.1. HREM studies of samples prepared by aqueous impregnation

Fig. 1 shows two HREM views representative of the nanostructure of the catalyst sample prepared by aqueous impregnation and further reduced at 473 K in a flow of hydrogen. It is worth mentioning that metal particles are not evident in these images, neither by visual inspection nor by the analysis of the DDP
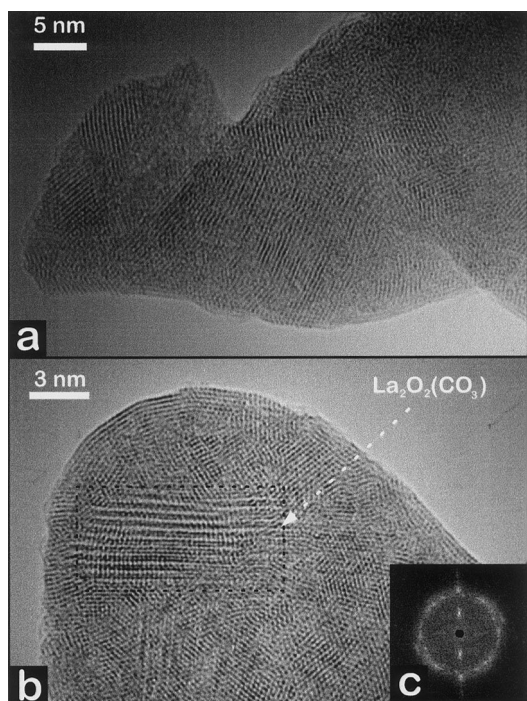
Fig. 1. (a) and (b) HREM images depicting the structure of the 10% Rh/La$_2$O$_3$ catalysts reduced at 473 K; (c) DDP calculated from a 512×512 pixel region of (b).

recorded from different areas in them. The high rhodium loading of this catalyst (10%), and the low surface area of the support, would suggest that rhodium particles should be easily detected. In this regard, we should remind that, according to previous image simulation studies [46,47], it is expected that metal particles about 1 nm size or bigger can be clearly detected in high resolution microscopes operating with experimental parameters like those used in this study. That was the case for other catalysts with lower nominal concentration of Rh atoms per square nanometer studied in our lab. Thus, the typical appearance of Rh/CeO$_2$ [37,38,40–43,45,46] and Rh/TiO$_2$ [36,37] catalysts containing a metal loading equivalent to 15 Rh atoms per square nanometer, after low temperature reduction, is that showing a high concentration of fairly well dispersed particles on the surface of the oxide supports. For the case of the Rh/La$_2$O$_3$ catalyst considered here the nominal rhodium concentration expected on the surface would be 60 atoms/nm^2. This value is equivalent to four monolayers of densely packed Rh atoms fully coating the surface of

the support or, from the point of view of a particle system, to one 0.8 nm in diameter Rh particle per square nanometer all over the catalyst surface. Such a large density of particles with a size within the detectable limit should be easily recognized in the experimental recordings. The calculations performed in [46,47] on structural models which include support oxides heavier than La$_2$O$_3$ rule out the possibility that the failure to detect metal particles in the images could be due to intrinsic limitations of the HREM technique. On the other hand, the analysis of low magnification TEM and SEM images of the same sample allows to conclude that the metal is not present in the form of very big particles which could skip to the view of the observer focussed in the recording of high magnification images.

A second aspect to be commented on the images included in Fig. 1 is that the catalyst particles are apparently constituted by an ensemble of very small crystallites, with an almost random relative orientation. The observation of a ring of reflections in the DDP included as Fig. 1(c), which was computed from a large region of the image, confirms further this idea. During the analysis of a large number of DDP corresponding to this sample, lattice spacings characteristic of lanthanum hydroxide, hydroxicarbonate and dioxomonocarbonate have been identified. In the particular case of the DDP shown in Fig. 1(c) the (0 0 2) reflections of type II-La$_2$O$_2$(CO$_3$) at 0.78 nm can be observed at low diffraction angles. The spacings that can be measured in the outer ring fall within the 3.4 Å range, in which all the hydrated/carbonated phases mentioned above present particular reflections. These results are in good correspondence with previous studies dealing with the chemical nature of the phases appearing in the successive preparation steps of this catalyst [20,22–26].

After the puzzling observation of the lack of features evidencing or suggesting the presence of any rhodium phase in the HREM images of the catalyst reduced at 473 K, several other treatments were essayed, addressed to detect the presence of the metal and to find reasonable tracks to clarify its microstructural evolution in parallel with treatments.

For this purpose, reduction treatments at increasing temperatures were applied in order to induce metal sintering. Thus, Fig. 2 shows HREM images depicting the structure of the 10% Rh/lanthana catalyst reduced
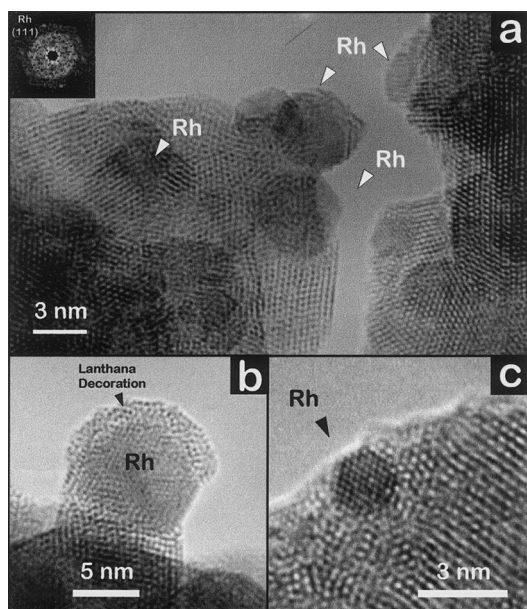
Fig. 2. (a) HREM image showing a general view of the 10% Rh/La$_2$O$_3$ catalyst reduced at 773 K. The DDP inset in the upper left was obtained from one of the small particles observed in this figure; (b) HREM detail of the same catalyst showing a Rh particle decorated by a lanthana overlayer; (c) HREM detail showing a 2 nm Rh particle on a lanthana background.

in a flow of hydrogen at 773 K. As a first general comment, it can be noted the presence of some Rh particles with diameters ranging from 2 to 10 nm. Nevertheless, the population of observable particles in these micrographs remains lower than that expected for samples loaded with the equivalent to four monolayers of Rh. An analysis of the digital diffraction patterns recorded in several selected areas show that metallic Rh is the only crystallographic phase containing the metal, and that after this thermochemical treatment, the support is now mainly constituted by La$_2$O$_3$. Some, rather scarce, lattice spacing typical of La(OH)$_3$ observed in small isolated regions could be attributed to the fast aging of the sample due to exposure to air during the transfer from the microreactor where it was prepared to the microscope specimen chamber.

Focussing now the attention in the profiles of the images, it is evident that most of the metal particles appear covered by patches of material which, according to their spacings, could be assigned to the support.

This decoration effect can be observed in detail in Fig. 2(b). To complete the comments of this figure, the idea that the different images clearly indicate that, for the case of the Rh/Lanthana system, metal particles can be evidenced both in profiles, Fig. 2(a) and (b), and in planar view, Fig. 2(c) should be stressed. In fact, this last image shows a very small and well faceted rhodium particle, probably embedded, or at least decorated, by the support. This observation is in good agreement with the image calculations referred in previous paragraphs and sheds light on previous reports in the literature disregarding the possibility of studying, by electron microscopy techniques, metals dispersed on rare earth oxides due to what the authors call lack of metal–support contrast [17].

Fig. 3(a) and (b) show, respectively, a low magnification view and a HREM detail of the structure of the 10% Rh/lanthana catalyst after reduction at 973 K. The aim of this treatment was trying to evidence if the population and/or size of the metal particles increased as to reach a more reasonable correspondence with the
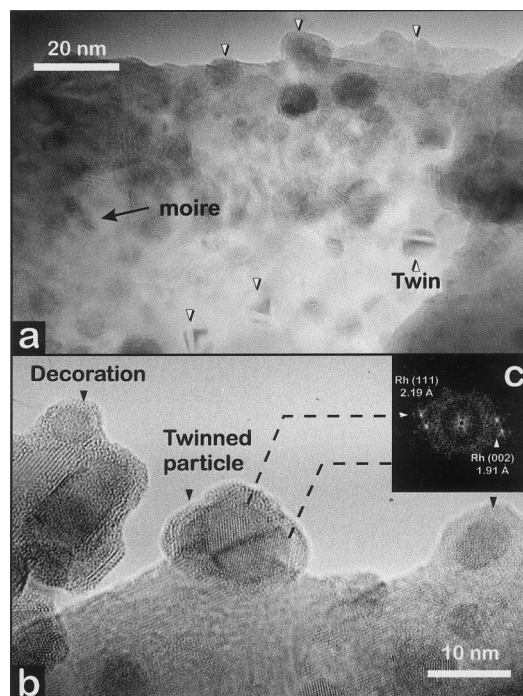
Fig. 3. (a) and (b) HREM images corresponding to the 10% Rh/La$_2$O$_3$ catalyst after reduction at 973 K; (c) DDP obtained from the lanthana-encapsulated Rh particle indicated in (b).

nominal metal content. Though such a point is difficult to conclude unequivocally, nevertheless an apparent increase of the metal present in the catalyst is now clearly evidenced by HREM. The amount of visible metal reaches levels that could be considered, on the basis of an estimation of the metal particle size distribution and the density of metal particles, as compatible with the loading of the catalyst.

Some other features of these micrographs deserve also a comment. First, the average size of the metal particle increases significantly. This fact and the data commented above indicate that, under the referred conditions, lanthana does not seem to have an inherent ability to maintain the metal in a highly dispersed state.

Second, a significant fraction of the metal particles, in particular of the bigger ones, appear twinned. Those marked with dark arrows in Fig. 3(a) are examples. The twinning effect is evidenced in DDPs as that in Fig. 3(c), which shows (0 0 2) spots at 0.191 nm coming from one of the twinned domains and (1 1 1) spots at 0.219 nm coming from a second one. The angle expected between these family of planes in a single crystal is about $55°$, a value much larger than that observed experimentally in the DDP. Twinning is considered in the literature as an usual mechanism of stabilization of metal crystallites.

Third, most of the surface of the metal particles which are observed on the edges remain covered by support material, as already noted for reduction treatments at 773 K.

In addition to the features commented in previous paragraphs, the presence of large spacing fringes is evident in different areas of Fig. 3(a). These fringes can be suitably and quantitatively interpreted as Moirè fringes appearing as a result of a double diffraction process in the catalyst. Moire patterns are common in plan-view TEM images, or SAED patterns, of systems with more than one component [52], as is the case of supported metal catalysts. Electron diffraction is usually so strong that the diffracted beams produced by the primary scattering process at the metal particles are intense enough to behave as incident beams on the underlying support crystallites. A second diffraction process brings the diffracted beams to low diffraction angles, and this gives rise to the large spacing fringes observed in the HREM images. Thus, the formation of new phases can be ruled out as the origin of these

fringe patterns. The increase of support crystallinity and metal particle size produced by the increase of reduction temperature favors to a large extent the intensity of the Moire effects.

In order to ascertain to what an extent the nano-structural changes observed upon increasing the reduction temperature were linked solely to thermal effects or to the simultaneous action of temperature and chemical surrounding during the treatment, a sample of the 10% Rh/lanthana catalyst was submitted to a reduction treatment at 773 K and further heated in a flow of helium at high temperature (1200 K). Fig. 4 shows a general view (a) and a high resolution detail (b) of this sample. A high density of rather large and well-faceted particles sitting on the surface of the support and covered by a thick layer of a distinct nature are also visible in these images. From the analysis of the DDP obtained from the particles, Fig. 4(c), it can be concluded that, after this treatment,
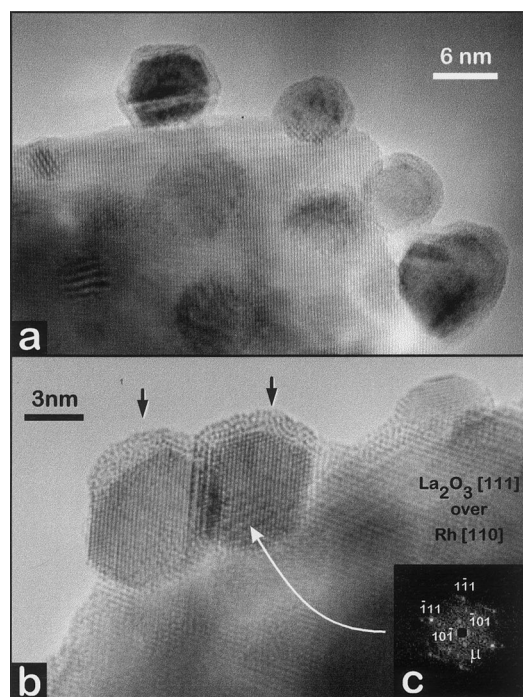
Fig. 4. (a) General view showing the structure of the 10% Rh/La$_2$O$_3$ reduced at 773 K and further heated in helium up to 1173 K; (b) HREM detail showing the presence of Rh particles decorated by thick lanthana overlayers; (c) DDP obtained from one of the particles seen in (b). Reflections coming from the Rh-[1 1 0] and La$_2$O$_3$-[1 1 1] zone axes are identified.

Rh remains in the metallic state. The presence of {1 1 1} and {0 0 2} reflections characteristic of f.c.c. Rh allows to assign this DDP to the [1 1 0] zone axis of rhodium. Some extra reflections, marked as $(1\,0 - \bar{1})$ and $(-1\,0\,\bar{1})$, which come from the thick support overlayer are also visible and can be assigned to the [1 1 1] zone axis of hexagonal La_2O_3. Moreover a moirè spot, marked in the DDP as μ, is also visible close to the center of the pattern. This reflection, which results from the combination of the $(1 - \bar{1}\,1)$-Rh and $(-\bar{1}\,0\,1)$-La_2O_3 ones, is due to double diffraction between either the support overlayer and the metal particles or the particle and the underlying lanthana crystallite.

A final HREM study undertook for the 10% Rh/ lanthana sample prepared by aqueous impregnation was related to a treatment which involved a direct heat treatment of the as prepared impregnated sample in a flow of helium up to 1200 K. This preparation resembles to the former one but in this case the reduction step in hydrogen was eliminated. The HREM images corresponding to this sample, Fig. 5(a), indicate the formation of very large, well-faceted, and clean orthorhombic-$LaRhO_3$ crystals mixed with La_2O_3 crystals. Thus the DDP obtained from the big particle contained in Fig. 5(a) could be assigned to the [0 1 0] zone axis of this perowskite type mixed oxide. The spot at 0.563 nm is that characteristic of the (0 0 1) planes of this phase, whereas that at 0.543 nm corresponds to the (1 0 0) set. Image simulation was performed to check this interpretation. Fig. 5(b) shows a HREM image calculated for a $LaRhO_3$ crystal, 10 nm thick, close to the [0 1 0] zone axis. In the DDP calculated for this simulation the (0 0 1) and (1 0 0) spots of the perowskite which are observed experimentally are nicely reproduced. This result provides further support to the phase assignment proposed above. Furthermore, XRD diagrams recorded for the sample heated directly in helium also reveal the presence of both phases, Fig. 6(a). It is also interesting to note with regard to the XRD experiments that a second XRD diagram recorded 5 days later, during which the sample was just exposed to air at room temperature, shows only peaks corresponding to $LaRhO_3$ and $La(OH)_3$, Fig. 6(b). The intensity of the main lanthanum rhodate peak suggests, in agreement with the HREM micrographs, that most, if not all, of the rhodium added to the catalyst has incorpo-
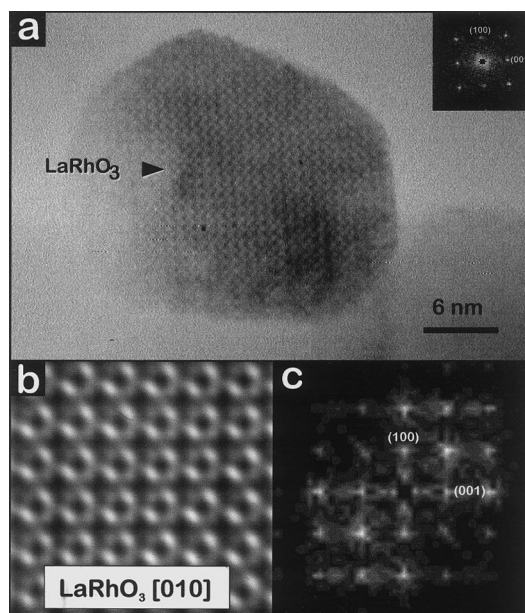
Fig. 5. (a) HREM obtained from the 10% Rh/La_2O_3 catalyst after a direct heat treatment under He up to 1200 K. The DDP inset on the upper right corner can be indexed as due to the [0 1 0] zone axis of a $LaRhO_3$ phase; (b) HREM simulated image corresponding to a 10 nm thick $LaRhO_3$ crystal 7° off the [0 1 0] zone axis. Tilting effect was included in the calculation in order to activate the {0 0 1} and {1 0 0} kinematic extinctions; (c) DDP obtained from the calculation shown in (b).

rated into the perowskite phase. Given that the reduction of rhodium sesquioxide in inert gas flow should occur below 1200 K, this result suggests that lanthana play a significant role stabilizing the rhodium atoms in the oxidized state.

To summarize the set of results obtained for the 10% Rh/lanthana catalysts, HREM suggests that at low reduction temperature the metal phase is in a highly dispersed state, with metal particles whose size must be of the order of a few angstroms. Burial of metal atoms within the support bulk is most likely. Increasing the reduction temperature induces severe sintering but the amount of visible metal is far from that expected for the total loading. Only treatments at very high temperature, either directly under hydrogen or under helium after a mild reduction are capable of producing a distribution of metal particles with reasonable sizes and surface density. In the range 773–1200 K surface decoration and complete encapsula-
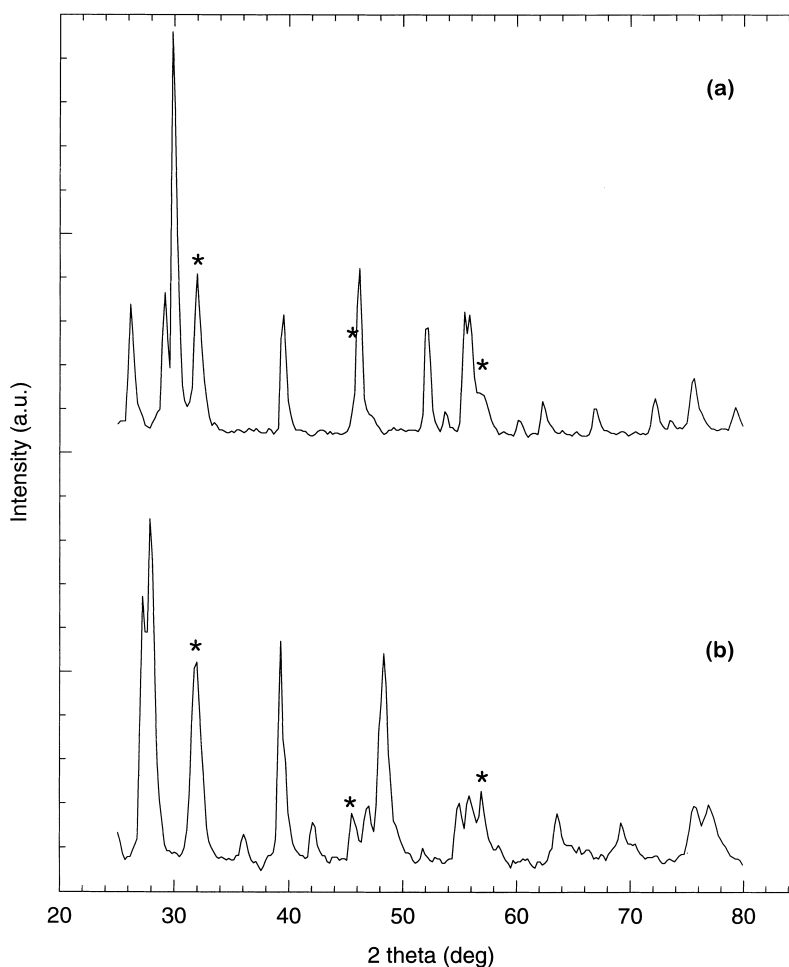
Fig. 6. (a) XRD diagram recorded on the 10% Rh/La_2O_3 catalyst heating under He up to 1200 K. Asterisks mark the position of the peaks characteristic of the lanthanum rhodate phase. The diagram was obtained just after the heat treatment; (b) diagram corresponding to the same sample after five days of exposure to air at room temperature. Note that $LaRhO_3$ peaks are still present mixed with those due to a $La(OH)_3$ phase.

tion of the metal particles by support material is observed, though such an effect cannot be disregarded for treatments at lower temperatures. The effect of high temperature treatments is quite different when the reduction of rhodium is circumvented. Thus direct heating in helium drives the system to the formation of lanthanum rhodate particles in which rhodium is stabilized in an oxidized state. This result points out to an intimate contact between Rh and La after the impregnation step, what, on the other hand, is in good agreement with the high dispersion state observed after low temperature reduction treatments. Comple-

mentary characterization data shown below, also support this idea.

3.2. Influence of the impregnation in the support crystallites morphology

As following impregnation with aqueous solutions of rhodium nitrate the metal was only detected after a severe reduction treatment, it was considered of interest to obtain more detailed information about the structural changes taking place in the system during the impregnation process. With this aim, the texture
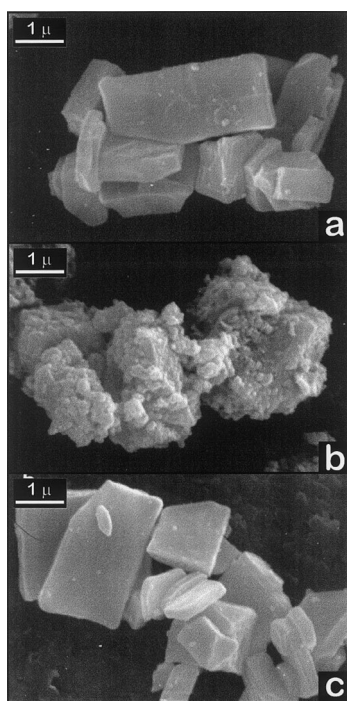
Fig. 7. (a) SEM image corresponding to the Y_2O_3 support; (b) SEM image obtained on the yttria sample after impregnation with an aqueous $Rh(NO_3)_3$ solution; (c) SEM image recorded after the impregnation of yttria with a solution of $Rh(NO_3)_3$ in acetone.

evolution of the support oxide was investigated by means of scanning electron microscopy (SEM).

For this study lanthana itself was not considered a good choice due to the rough nature of its particles which would prevent a clear observation of any possible morphological change during the impregnation process. For that reason a Y_2O_3 sample, which is in fact an oxide with chemical properties not too far from those of lanthana and available in the form of well shaped crystallites was selected. The secondary electron image presented in Fig. 7(a) shows that this yttria sample is constituted by micron sized, prismatic like, aggregates with a low apparent roughness.

As depicted in Fig. 7(b), after impregnation with the rhodium nitrate aqueous solution, the texture of this sample changes dramatically. The yttria grains appear very rough now, and a huge amount of sub-micron pieces is also present. Extensive dissolution of the oxide by the impregnating solution must be responsible of such a dramatic transformation. This

dissolution process could proceed through the reaction of the acid impregnation solution with the markedly basic yttria support. Latter re-precipitation of lanthana and rhodium during the drying step would give rise to the small crystallites appreciated in the SEM images.

On the contrary, when the impregnation step is carried out with rhodium nitrate solutions in acetone any change in the morphology of the support particles, at least at the micrometer level, can hardly be noted, Fig. 7(c). Some chemical dissolution essays with acidified acetone solutions proved that the solubility of lanthana in such media is very low.

Thus, the above results show to what extent the dissolution effects can dramatically affect to the preparation of dispersed metals on rare earth sesquioxides. If we compare the basicity of yttria with that of lanthana, it would be higher for the latter; this suggesting that the influence of the aqueous impregnation treatment of lanthana support would be critical in the preparation of the sample and its further behavior.

3.3. HREM studies of samples prepared by impregnation with acetone solution

Fig. 8 shows a general view (a) and a HREM close up of the 8% Rh/lanthana sample prepared by impregnating the support with rhodium nitrate solutions in acetone, after reduction at low temperature, 473 K.

In the general overview, a large density of very small particles, most of them slightly larger than 1 nm in size, can be appreciated in planar view. According to the SAED pattern shown as Fig. 9, such particles correspond to metallic rhodium. This is revealed by the diffraction ring at 0.219 nm, characteristic of the {1 1 1} planes of this f.c.c. type metal. The coexistence of ultradispersed rhodium particles undetectable by HREM cannot be disregarded anyway. Though metal particles are not visible in the profiles, in this case we can at least observe a significant fraction of the rhodium loaded on the catalysts. This clearly contrasts with the results obtained for the catalyst prepared via aqueous impregnation at the same reduction temperature.

The structure of the support is, nevertheless, similar to that observed for the 10% Rh/lanthana catalysts. Thus, the image in Fig. 8(b) shows the intricate pattern of lattice fringe patches, disposed in a more or less
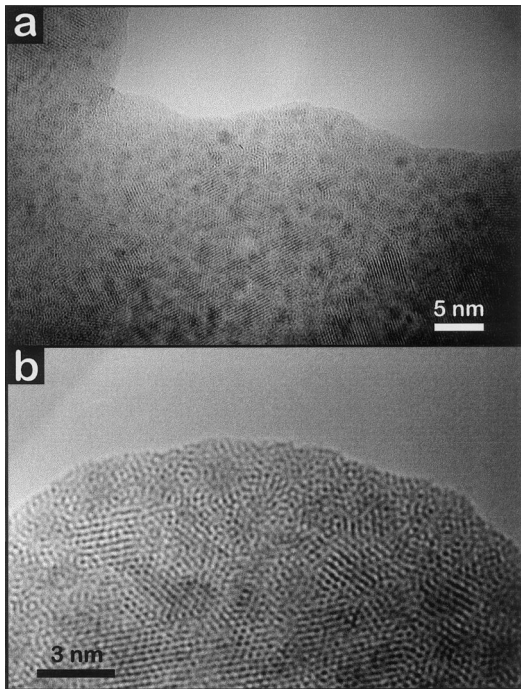
Fig. 8. General view (a) and HREM detail (b) of the 8% Rh/La$_2$O$_3$ catalyst, prepared with acetone solution, after a reduction treatment at 473 K.

random orientation, which is typical of aged lanthana. Careful analysis of DDP indicates the presence of hydroxicarbonated phases.
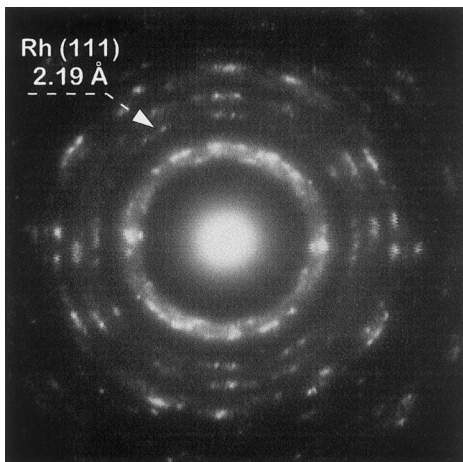
Fig. 9. SAED pattern recorded on the 8% Rh/La$_2$O$_3$ catalyst reduced at 473 K. The position of a ring of Rh {1 1 1} reflections has been marked.
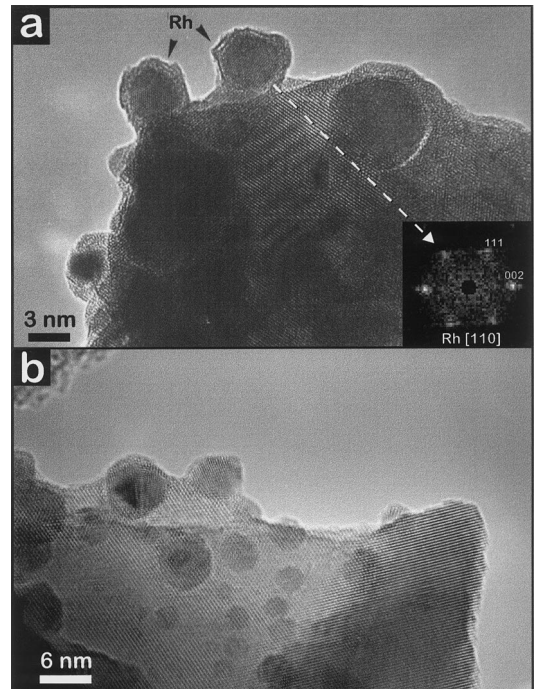
Fig. 10. Two HREM images representative of the 8% Rh/La$_2$O$_3$ catalyst reduced at 773 K. The DDP inset in figure (a) was obtained from the particle marked in that figure.

HREM micrographs corresponding to the reduction of this 8% Rh/lanthana sample at 773 K, Fig. 10, are characterized by a high apparent concentration of large metal particles showing evidences of extensive decoration by support material.

When similarities with the formerly studied samples are sought, the catalyst prepared by aqueous impregnation reduced at 973 K is that showing the closest microstructure. Given that lanthana dissolution effects in acetone are negligible, the origin of the decoration effect and metal particles growth in this sample must be the result of the transformations taking place during the reduction process, in the range of temperatures between 473 and 773 K.

3.4. HREM studies of samples prepared by rhodium evaporation on lanthana

Evaporation procedures should lead directly to the deposition of metallic particles on the substrate, without the need of further chemical treatments [49,53].
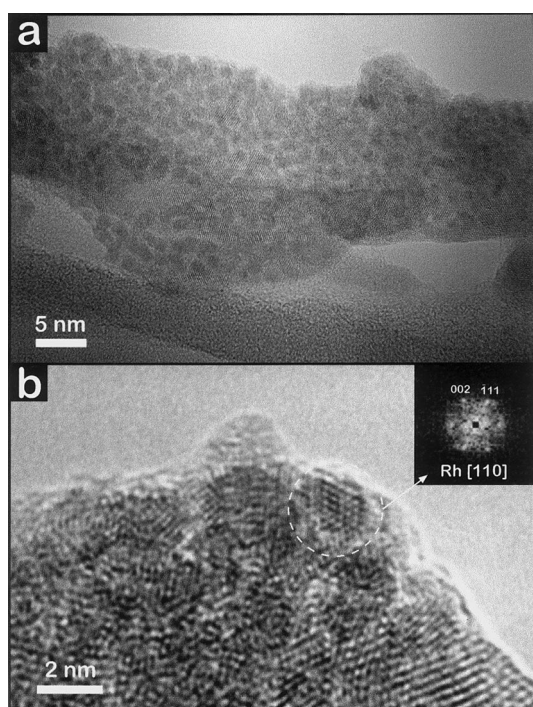
Fig. 11. General view (a) and HREM detail (b) of the Rh/La$_2$O$_3$ catalyst prepared by vacuum deposition, after reduction at 473 K. DDP analysis, inset in (b), indicate the existence of metallic Rh particles.

Fig. 12. General view (a) and HREM detail (b) of the Rh/La$_2$O$_3$ catalyst prepared by vaccum deposition, after reduction at 773 K. Large Rh particles decorated by lanthana are observed.

Nevertheless, in order to reach comparative sample states and, also, to be able to study the influence of reduction temperature, the as-prepared Rh/lanthana sample was treated in hydrogen at the same temperatures employed in the previous studies carried out on the catalysts prepared by wet routes.

Fig. 11(a) shows a general view image of the Rh/lanthana catalysts prepared by metal evaporation after reduction at 473 K. The spotty appearance of the crystal contained in this image resembles that observed in Fig. 9 for the catalyst prepared in acetone after low reduction temperature. In this case we can observe the support surface densely populated by small Rh particles. DDP analysis performed on small regions of HREM images, Fig. 11(b), indicates the presence of metallic rhodium particles. Thus, a high density of nanometer sized Rh clusters is the responsible for the contrasts observed in Fig. 11(a).

Increasing the reduction temperature up to 773 K leads to sintering of the metal particles, Fig. 12(a); a

significant fraction of which shows complete or partial decoration effects, as that in Fig. 12(b).

4. Discussion

Most of the authors working on rare earth sesqui-oxides as catalyst supports have noted singularities in their behavior and have contributed to define micro-structural models in which such singularities could be reasonably explained. Nevertheless, most of the applied characterization techniques have not provided direct structural data which allow to validate the proposed models.

To our knowledge, HREM has not been profitably used for this aim and, in fact, some misleading concepts regarding the lack of adequacy of the technique to the problem have been spread in the literature. For these reasons, the general purpose of this paper is to discuss on the one side the limitations, and on the other

side the contributions, that HREM can offer for a better understanding of these systems.

The summary of facts shown in Section 3 which can help to reach a better definition of nanostructural models for these catalysts would be the following:

1. Metal particles could not be observed in the sample prepared by aqueous impregnation reduced at 473 K, regardless of its high metal content.
2. The impregnation with an aqueous solution of metal precursor salt produces a severe support dissolution effect. For the case of a high loading rhodium sample prepared from a nitrate precursor the effect on the morphology of the particles is devastating.
3. The sample prepared by aqueous impregnation treated in inert gas at very high temperature forms a perowskite phase, thus stabilizing the metal in a dispersed oxidized state.
4. The size of the Rh particles does not seem particularly stabilized by the support. Thus, apparently the particle size increases gradually with the reduction temperature.
5. There is a clear tendency for the large metal particles to appear covered by support patches. Thus, when the reduction temperature is 773 K or higher, each of the samples seems to present a pattern of behavior not far from those of the others.

One of the reasons that could explain the absence of metal particles in the sample prepared by aqueous impregnation when reduced at 473 K could be an incomplete reduction of the metal. Nevertheless, both the general data available from the literature for noble metals dispersed on lanthana, and those obtained in our laboratory for this sample, suggest more likely that most of the metal would be in a reduced state. Thus, Kuznetsov et al. [54] observe by XPS that Pd or Rh precursors on lanthana start their reduction at 393 K, and become fully reduced at 413 K. Van der Lee et al. [7] have proposed the use of acetonitrile in acetil acetone to dissolve quantitatively the fraction of oxidized rhodium in a Rh/lanthana catalyst. The percentage of extracted rhodium following a reduction at 473 K was lower than 10%. In [55,56] a reduction treatment at 448 K is supposed to lead to the full reduction of Pd precursors deposited on rare earth

sesquioxides. Gallaher et al. [17,18] conclude that a Rh/lanthana catalyst has reached its full reduction after treatment in a flow of hydrogen at 473 K. Among the evidences of low temperature reduction of Rh obtained in our laboratory [20,22–26] we can mention: the observation of strong water signals associated to hydrogen consumption in TPR experiments for the temperature range 373–473 K, activated reduction of carbonates to CO and CH_4 starting from 373 K which are assumed to be related to the formation of dispersed metal, weight losses by TG analysis in a flow of hydrogen between 400 and 473 K not observed for inert gas treatments, elimination of IR signals corresponding to nitrate species, and significant hydrogen adsorption.

It is also important to note that the H_2 and CO chemisorption properties of the Rh/lanthana catalyst prepared by aqueous impregnation show some singular features which are similar to those reported for other noble metal supported on lanthana catalysts. Thus, the H_2 chemisorption capability of the sample prepared using the aqueous solution leads to apparent dispersion values decreasing from 55% at 623 K to 35% at 773 K [20]. Nevertheless, from CO chemisorption the apparent dispersion is only 5%. This inhibition of the CO adsorption with respect to the hydrogen adsorption, is a common feature also reported for other metal/lanthana catalysts [10,12,16]. It suggests that the nanostructural aspects governing the chemisorption behavior should be similar for preparations containing different noble metals and carried out in different laboratories.

The models proposed up to now in the literature for metals dispersed on lanthana assume that the metal particles are covered by lanthana patches [15–18]. The decoration effects have been attributed to reduction of the support followed by its migration [15,16], or alternatively, to dissolution effects in the impregnation process followed by reprecipitation [10,17,18,48]. The HREM and SEM results reported herein suggest that the impregnation step with the aqueous acidic solution containing the precursor must dissolve the support in a very significant way. Previous results showing the leaching effect on lanthana of the impregnation with an aqueous solution of rhodium chloride showed that the support reacted with the impregnating solution up to a point in which it was neutralized [26]. With this in mind we can understand that the trans-

formations of the support were as severe as suggested by the SEM results. After drying, most of the metal atoms would remain embedded in the bulk of the support at a very high level of dispersion. The high diffusivity of hydrogen would allow it to penetrate into the bulk of the impregnated sample and reduce the metal at temperatures lower than 473 K, as suggested by all the above described evidences. It can be also proposed that the metal in such state of dispersion in the bulk retains to some extent the capability for hydrogen sorption, though CO cannot diffuse to reach the encapsulated metal. The occurrence of hydrogen spillover from a small fraction of Rh atoms present on the surface of this highly dispersed phase to the neighboring support could alternatively explain the differences found between hydrogen and CO chemisorption. This idea would be in good agreement with DTP-H_2 diagrams obtained on different Rh/La_2O_3 [20] and Rh/Sm_2O_3 [19] catalysts which indicate the presence of several high temperature hydrogen forms that should be associated with hydrogen adsorption on these oxides.

When the reduction temperature increases up to 773 K the support undergoes a deep rearrangement as a result of its transformation from an hydroxycarbonated phase to lanthanum sesquioxide. It is well known that such a rearrangement takes place in several steps. Each of these steps offers to lanthana and also to the dispersed metal an opportunity to decrease its free energy. The mobility of the support during this phase transformations could favor its migration on top of the metal particles. In other words, support dehydration and decarbonation seems to be the driving force for the decoration process. In the catalysts prepared by aqueous impregnation a close contact between rhodium and the support exists from the early stages of the preparation procedure, in what case the support present on the particles could be just material dragged by the metal during the sintering process.

According to the characterization studies carried out recently on Ni/lanthana catalysts, the carbonated phases of lanthana could play also a direct role in the catalytic cycle of the dry reforming of methane. Thus in [28,29] it is shown that the exposure of a Ni/La_2O_3 catalyst to the stream of reactants at 750°C, leads to the formation of $La_2O_2CO_3$. It is also proposed that the decomposition of this phase provides a route to convert CO_2 into CO and, at the same time, eliminate the carbon species deposited onto the surface of nickel during the cracking of methane. This assumption suggests the existence of high mobility in the support under the actual catalytic reaction conditions. The tendency of the support to get in contact with the metal after its decomposition, revealed in the present study, in parallel with the formation/decomposition of $La_2O_2CO_3$ during the dry reforming of methane could lead to a continuous increase of the coverage of the metal particles during the first hours of reaction. After this period, an optimum coverage value could be reached which would explain the stationary activity regime observed experimentally.

5. Conclusions

Different particular conclusions have already been outlined in appropriate points of Sections 3 and 4, so here only general remarks about the original contributions of this work will be mentioned.

One of the remarkable conclusions of the present work is that, contrary to the general opinion currently established in the literature, high resolution electron microscopy is a very suitable technique to characterize in detail the nanostructure of metal catalysts supported on heavy oxides, as is the case of lanthana. Both profile and planar view images can be recorded and exploited to gain information about the structural evolution of this family of catalysts with chemical and thermal treatments. In particular, the images and electron diffraction patterns obtained in this work have allowed us to understand the influence of the preparation procedure on the catalyst structure. Thus, the strong modifications induced by the impregnation treatments with aqueous solution, both on the texture and the metal dispersion state, have been evidenced.

A model to understand the peculiar chemisorption properties and the origin of the metal particle decoration phenomena has been proposed. In contrast with previous models, in this case the existence of a highly dispersed phase after impregnation and reduction at low temperature is assumed. Mixing of Rh^{3+} species present in aqueous solution with the support dissolved during the impregnation would provide the means to create a framework where most of the Rh ions would be likely dispersed in the bulk of the impregnated phase. This model invokes chemical properties well

established for the 4f-sesquioxides as it is their basicity and the thermochemical behavior of their hydrated-carbonated phases. The reduction of lanthana at 773 K to suboxide species claimed by other authors, in an extrapolation of the model proposed for the SMSI effect in metal/TiO$_2$ catalysts, has been avoided. Such extrapolation should in fact be considered rather daring if the well known low reducibility of lanthana is taken into consideration.

Acknowledgements

References

[1] R.F. Hicks, A.T. Bell, J. Catal. 90 (1984) 205.

[2] R.F. Hicks, A.T. Bell, J. Catal. 91 (1985) 104.

[3] C. Sudhakar, M.A. Vannice, J. Catal. 95 (1985) 227.

[4] J.S. Rieck, A.T. Bell, J. Catal. 96 (1986) 88.

[5] M.A. Vannice, C. Sudhakar, M. Freeman, J. Catal. 108 (1987) 97.

[6] F. Le Normand, J. Barrault, J. Breault, R. Breault, L. Hilaire, A. Kiennemann, J. Phys. Chem. 95 (1991) 257.

[7] G. Van der Lee, B. Schuller, H. Post, T.L.F. Favre, V. Ponec, J. Catal. 98 (1986) 522.

[8] R.P. Underwood, A.T. Bell, Appl. Catal. 21 (1986) 157.

[9] N.K. Pande, A.T. Bell, J. Catal. 98 (1986) 1.

[10] R.P. Underwood, A.T. Bell, Appl. Catal. 34 (1987) 289.

[11] D. Yu-Hua, C. De-Au, T. Khi Rui, Appl. Catal. 35 (1987) 77.

[12] R.P. Underwood, A.T. Bell, J. Catal. 109 (1988) 61.

[13] R.P. Underwood, A.T. Bell, J. Catal. 111 (1988) 325.

[14] L. Bruce, S. Hardin, M. Hoang, T. Turkey, Stud. Surf. Sci. Catal. 36 (1988) 529.

[15] T.H. Fleisch, R.F. Hick, A.T. Bell, J. Catal. 87 (1984) 398.

[16] R.F. Hick, Q.J. Yen, A.T. Bell, J. Catal. 89 (1984) 498.

[17] G. Gallaher, J.G. Goodwin Jr., C.S. Huang, M. Houalla, J. Catal. 127 (1991) 719.

[18] G. Gallaher, J.G. Goodwin Jr., L. Guczi, Appl. Catal. 73 (1991) 1.

[19] S. Bernal, F.J. Botana, J.J. Calvino, G.A. Cifredo, J.M. Rodríguez-Izquierdo, Eur. J. Solid State Inorg. Chem. 28 (1991) 441.

[20] S. Bernal, F.J. Botana, R. García, F. Ramírez, J.M. Rodríguez-Izquierdo, in: C. Morterra, A. Zecchina, G. Costa (Eds.), Structure and Reactivity of Surfaces, 1989, p. 123.

[21] D.K. Smith, J. Chem. Ed. 63 (1983) 228.

[22] S. Bernal, E. Blanco, F.J. Botana, R. García, F. Ramírez, J.M. Rodríguez-Izquierdo, Mater. Chem. Phys. 17 (1987) 433.

[23] S. Bernal, F.J. Botana, R. García, F. Ramírez, J.M. Rodríguez-Izquierdo, Appl. Catal. 31 (1987) 267.

[24] S. Bernal, F.J. Botana, R. García, F. Ramírez, J.M. Rodríguez-Izquierdo, Chem. Soc., Faraday Trans. 83(8) (1987) 2279.

[25] S. Bernal, F.J. Botana, R. García, F. Ramírez, J.M. Rodríguez-Izquierdo, J. Mater. Sci. 22 (1987) 3793.

[26] R. Kieffer, M. Rodríguez, A. Kiennemann, J.M. Rodríguez-Izquierdo, S. Bernal, Appl. Catal. 42 (1988) 77.

[27] P. Gronchi, C. Mazzochia, R. Del Rosso, Energy Convers. Mgmt. 36(6–9) (1995) 605.

[28] Z. Zhang, X.E. Verykios, Appl. Catal. 138 (1996) 109.

[29] Z. Zhang, X.E. Verykios, S. Mac Donald, S. Affrossman, J. Phys. Chem. 100 (1996) 744.

[30] P. Gronchi, D. Fumagalli, R. Del Rosso, P. Centola, J. Thermal Anal. 47 (1996) 227.

[31] P. Gronchi, S. Marengo, C. Mazzochia, E. Tempesti, R. Del Rosso, React. Kinet. Catal. Lett. 60(1) (1997) 79.

[32] P. Gronchi, P. Centola, R. Del Rosso, Appl. Catal. A 152 (1997) 83.

[33] V.A. Tsipouriari, X.E. Verykios, J. Catal. 179 (1998) 292.

[34] A.D. Logan, E.J. Braunschweig, A.K. Datye, D.J. Smith, Langmuir 4 (1988) 827.

[35] E.J. Braunschweig, A.D. Logan, A.K. Datye, D.J. Smith, J. Catal. 118 (1989) 227.

[36] S. Bernal, F.J. Botana, J.J. Calvino, C. López, J.A. Pérez-Omil, J.M. Rodríguez-Izquierdo, J. Chem. Soc., Faraday Trans. 92(15) (1996) 2799.

[37] S. Bernal, J.J. Calvino, M.A. Cauqui, G.A. Cifredo, A. Jobacho, J.M. Rodríguez-Izquierdo, Appl. Catal. 99 (1993) 1.

[38] S. Bernal, F.J. Botana, R. García, Z. Kang, M.L. López, M. Pan, F. Ramírez, J.M. Rodríguez-Izquierdo, Catal. Today 2 (1988) 653.

[39] H.D. Cochrane, J.L. Hutchinson, D. White, G.M. Parkinson, C. Dupas, A.J. Scott, Ultramicroscopy 34 (1990) 10.

[40] S. Bernal, F.J. Botana, J.J. Calvino, M.A. Cauqui, G.A. Cifredo, A. Jobacho, J.M. Pintado, J.M. Rodríguez-Izquierdo, J. Phys. Chem. 97 (1993) 4118.

[41] S. Bernal, F.J. Botana, J.J. Calvino, G.A. Cifredo, J.A. Pérez-Omil, Proceedings of EMAG'93, Inst. Phys. Conf. Serv., vol. 138, Liverpool, UK, 1993, p. 485.

[42] S. Bernal, G. Blanco, J.J. Calvino, G.A. Cifredo, J.A. Pérez-Omil, J.M. Pintado, A. Varo, Stud. Surf. Sci. Catal. 82 (1994) 507.

[43] S. Bernal, F.J. Botana, J.J. Calvino, G.A. Cifredo, J.A. Pérez-Omil, J.M. Pintado, Catal. Today 23 (1995) 219.

[44] A.K. Datye, D.S. Kalakkad, M.H. Yao, D.J. Smith, J. Catal. 155 (1995) 148.

[45] S. Bernal, J.J. Calvino, J.M. Gatica, C. Larese, C. López-Cartes, J.A. Pérez-Omil, J. Catal. 109 (1997) 510.

[46] S. Bernal, F.J. Botana, J.J. Calvino, C. López-Cartes, J.A. Pérez-Omil, J.M. Rodríguez-Izquierdo, Ultramicroscopy 72 (1998) 135.

[47] S. Bernal, J.J. Calvino, M.A. Cauqui, J.A. Pérez-Omil, J.M. Pintado, J.M. Rodríguez-Izquierdo, Appl. Catal. B 16 (1998) 127.

[48] S. Bernal, F.J. Botana, J.J. Calvino, G.A. Cifredo, R. García, J.M. Rodríguez-Izquierdo, Ultramicroscopy 34 (1990) 60.

[49] G. Rupprechter, K. Hayek, H. Hofmeister, J. Catal. 173 (1998) 409.

[50] P. Stadelmann, Ultramicroscopy 21 (1987) 131.

[51] F.J. Botana, J.J. Calvino, G. Blanco, M. Marcos, J.A. Pérez-Omil, Electron Microscopy 1994 2B (1994) 1085.

[52] L. Reimer, Transmission Electron Microscopy, Springer, Berlin, 1984, pp. 333–336.

[53] G. Rupprechter, K. Hayek, L. Rendón, M.J. Yacamán, Thin Solid Films 260 (1995) 148.

[54] V.L. Kuznetsov, I.L. Mudrakowski, A.V. Romanenko, A.V. Pashis, V.M. Mastikhin, Y.I. Yermakov, React. Kinet. Catal. Lett. 25 (1984) 137.

[55] M.D. Mitchell, M.A. Vannice, Ind. Eng. Chem. Fundam. 23 (1984) 88.

[56] C. Sudhakar, M.A. Vannice, Appl. Catal. 14 (1985) 47.